Electromagnetic Field Enhancement for Wedge-Shaped Metal Nanostructures

ARTICLE *in* JOURNAL OF PHYSICAL CHEMISTRY LETTERS · JULY 2011

Impact Factor: 7.46 · DOI: 10.1021/jz200825g

3 AUTHORS, INCLUDING:

Ali Angulo Martínez
Instituto de Ciencias Nucleares
3 PUBLICATIONS **33** CITATIONS
SEE PROFILE

Cecilia Noguez
Universidad Nacional Autónoma de México
87 PUBLICATIONS **2,577** CITATIONS
SEE PROFILE

THE JOURNAL OF PHYSICAL CHEMISTRY Letters

LETTER

pubs.acs.org/JPCL

Electromagnetic Field Enhancement for Wedge-Shaped Metal Nanostructures

Ali M. Angulo,[†] Cecilia Noguez,*[,†] and George C. Schatz[‡]

[†]Instituto de Física, Universidad Nacional Autónoma de México, Apartado Postal 20-364, México D.F. 01000, México

[‡]Department of Chemistry, Northwestern University, Evanston, Illinois 60208, United States

ABSTRACT: The role of localized surface plasmon resonances near the surface of a silver or gold wedge is discussed based on quasistatic theory. Strongly enhanced electromagnetic field intensities at moderate distances of 1 nm from the wedge are found by manipulating morphology and dielectric environment. The theory also shows that wedge structures can have high enhancements over a broad range of wavelengths, which is of relevance to surface-enhanced Raman scattering and tip-enhanced Raman scattering measurements and for improving plasmon enhanced photovoltaic devices.

SECTION: Nanoparticles and Nanostructures

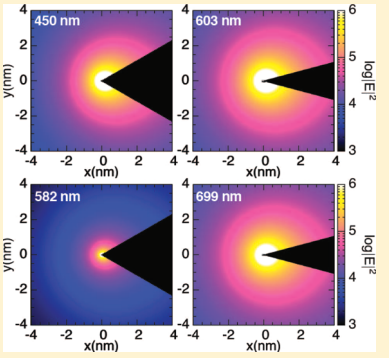

Interest in the optical properties of nanoparticles (NPs) arises from the large morphology-dependent physical properties of these systems. Metallic NPs strongly couple with light through excitation of surface plasmon resonances (SPRs), which are collective excitations of the electrons near the interface between a conductor and an insulator. This strong coupling leads to novel phenomena at the nanometer scale, including localization and consequent enhancement of the electromagnetic (EM) field that can be manipulated for transport and storage of energy,[1] significant increase in the sensitivity of sensors and spectroscopies,[2] enhanced optical forces for controlling the growth of NPs,[3,4] increased light absorption for improving photovoltaic devices,[5] photothermal destruction of cancer cells and pathogenic bacteria,[6,7] and many other technological applications. The SPRs of metal NPs can be tuned by controlling their size, shape, and environment, providing a starting point for emerging research fields based on plasmonics.[8] In many cases, the search for novel plasmonic structures is aimed at finding the particle or arrays of particles that produce the strongest local EM field enhancement. This enhancement increases the light absorption efficiency of plasmonic solar cells,[9] as well as the sensitivity of surface-enhanced Raman scattering (SERS).[2,10] It has been suggested that narrow gaps between NPs, as well as sharp corners, edges, and tips of metal NPs, can be useful for producing large enhancement factors.[11] Numerical simulations have shown SPRs localized near the metal surface of NPs with polygonal shapes such as decahedra, octahedra, and cubes.[12,13] However, the SPRs and thus the EM field enhancement on such structures are extremely sensitive to the local dielectric environment and morphology.[14]

One structure that provides a useful model for plasmonic behavior is a perfectly sharp wedge. This is one of the few problems in physics that admits to an analytical solution to the electrodynamics within the quasistatic limit, and it defines a zero radius of curvature structure that can be used to probe the extremes of EM enhancement effects. Of course the well-known field divergence that occurs at the tip of the wedge in the quasistatic limit is unphysical for describing real particle structures; however, the fields at positions removed from the tip (such as by atomic dimensions) are finite, and can therefore be used to provide physical insight about fields near tips. One feature of the perfect wedge is that it is an infinite sized object that can be used to model tip-enhanced Raman scattering (TERS). This stands in contrast to most electrodynamics studies of TERS, in which finite structures (with rounded tips) have been studied with electrodynamics methods.[15−20] The finiteness of the structures results in a dense series of multipole resonances whose properties are hard to relate to the experiments. A recent study demonstrated the capability of modeling an infinite tip using finite element methods,[21] but this leads to a complex calculation from which it is hard to provide qualitative insight. TERS has also been studied using simple analytical models such as with point dipoles or finite spheres,[22] and recently a quasistatic model was developed based on structures that are defined using prolate ellipsoidal coordinates.[23] The latter work provides an alternative approach to the wedge model for studying an infinite structure where analytical theory can be developed, and the results were used to provide qualitative insight about TERS, but with a structure that is fundamentally different from a wedge structure.

Received: June 17, 2011
Accepted: July 20, 2011

dx.doi.org/10.1021/jz200825g | *J. Phys. Chem. Lett.* 2011, 2, 1978–1983

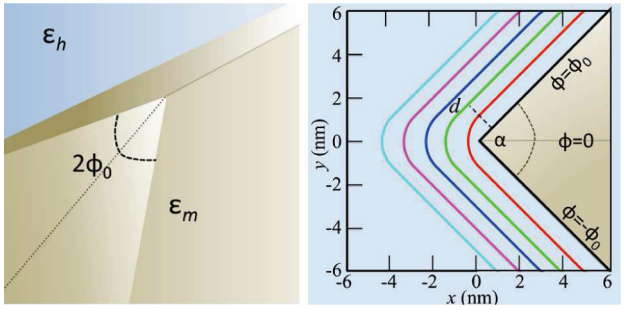

Figure 1. Schematic model (left) and cross section (right) of an infinite metal wedge. The color lines show different paths at fixed distances of d from 1 to 5 nm around the wedge.

In this paper we examine electric fields for the wedge structure, including models for both silver and gold wedges, with emphasis on the variation of the fields near the tip as a function of wedge angle, wavelength and dielectric constant of the surrounding medium. The results will be of particular use for understanding what wavelengths lead to maximum enhancements, which is an important issue in the design of TERS tips, and we also examine the spatial profile of the maximum field, which interestingly is not always located precisely at the tip position. Comparisons with earlier results will be provided, which calibrate the comparison of wedge results with accurate electrodynamics results for rounded tips.

Numerical solutions of this problem using the discrete dipole approximation (DDA) and finite-difference time-domain (FDTD) calculations are very time-consuming, and a systematic search for the best plasmonic nanostructure using these methods is almost impossible. In this paper, we employ an analytical expression that allows us to obtain an efficient algorithm for the systematic solution of the EM field, and is helpful for analyzing the obtained numerical solutions. In Figure 1, we show a schematic model of the cross section of the wedge, which consists of an infinite metallic wedge within the region $-\phi_0 \leq \phi \leq \phi_0$, of homogeneous material and dielectric function $\varepsilon_m(\omega)$, which is immersed in a homogeneous medium with dielectric constant ε_h within the region $\phi_0 \leq \phi \leq 2\pi - \phi_0$. We assume that the magnetic permeability is $\mu = 1$ in both regions. It is assumed that the structure is invariant along the z axis.

To solve the Maxwell equations for periodic fields with frequency ω in the presence of the wedge, we introduce the cylindrical coordinates ρ, ϕ, and z, with the z axis along the edge and ρ taken as the distance from the edge. We employ the quasistatic Meixner approach, valid for NPs that are 40 nm and smaller,[8] to study the local SPR on the wedge, where the solutions of the EM fields in both metal and dielectric have the form[24]

$$\begin{aligned} E_\rho &= \sum_{j=0,\infty} a_j \rho^{t-(1-j)}, & H_\rho &= \sum_{j=0,\infty} d_j \rho^{t-(1-j)} \\ E_\phi &= \sum_{j=0,\infty} b_j \rho^{t-(1-j)}, & H_\phi &= \sum_{j=0,\infty} f_j \rho^{t-(1-j)} \\ E_z &= \sum_{j=0,\infty} c_j \rho^{t-(1-j)}, & H_z &= \sum_{j=0,\infty} g_j \rho^{t-(1-j)} \end{aligned} \quad (1)$$

Here, a_j, b_j, c_j, and d_j, f_j, g_j are expansion coefficients that depend only on ϕ and z; and the parameter t is determined from the boundary conditions. It was shown that physical meaning solutions are found if the strengths of **E** and **H** are infinite at the edge, but with an integrable energy density in a finite region, which is known as the edge condition.[24] Then, it follows that $0 < \mathrm{Re}(t) < 1$, and $c_0 = g_0 = 0$. This means that the components of **E** and **H** parallel to the edge are finite, and then, the EM field is perpendicular to the transverse section. This corresponds to the transverse magnetic mode with a line dipole excitation. The solution studied here is consistent with the case of illumination by x-polarized incident light and not y-polarized incident light according to Figure 1, and consistent with other numerical results.[25] We restrict ourselves to the region very close to the wedge, i.e., for $\rho \ll \lambda$, where λ is the wavelength of the external EM field. In this case, the components E_ρ and E_ϕ are power functions with $t - 1$ indicating the power index of the singularity in the electric field. All other components have no singularities at the wedge.

Now, we follow the same procedure as Lapchuck et al. in ref 26 to find the solution of the above equations for real metals, in particular for silver (Ag) and gold (Au) NPs.[27] For details of the mathematical equations the reader can consult ref 26. They found that the boundary conditions at $\phi = \pm\phi_0$ and eqs 1 lead to the following expression:[26]

$$\frac{\varepsilon_h - \varepsilon_m(\omega)}{\varepsilon_h + \varepsilon_m(\omega)} = \pm \frac{\sin[\pi t]}{\sin[(\pi - 2\phi_0)t]} \quad (2)$$

Equivalent relations to the above equation have been obtained for electrostatic modes localized in the vicinity of the edge of a dielectric wedge using different coordinate systems and approaches.[28,29] From here, the resulting modes can be classified as even (+) or odd (−) under reflection in the plane bisecting the wedge.[30] Their frequencies are functions of the continuously varying parameter t. The solution, in the complex plane,[31] of the above equation yields t that describes the field singularity at the wedge. This power index is a complex parameter, $t = t_{re} + it_{im}$, that depends on the boundary conditions. For simplicity, we denote the internal angle of the wedge as $\alpha \equiv 2\phi_0$. Even and odd modes will always exist, independent of α, but the singularity exists for different modes for different ranges of α. From the edge condition it is followed that odd modes are found for angles $\alpha < 180°$ (wedge), while even modes are present when $\alpha > 180°$ (groove). Finally, we find that the electric field intensity relative to the incident field at small distances is given by

$$|E|^2 = \rho^{2(t_{re}-1)} \cosh[2t_{im}(\phi - \pi)] \quad (3)$$

This expression is composed of a function of the radial position, ρ, that shows the field singularity, which is stronger when $t_{re} \to 0$; and a function of ϕ, which is related to the symmetry of the field and depends on t_{im}, that takes values ≤ 0 and modulates how fast the field decays as a function of the angle. This factor is larger close to the wedge walls ($\phi \to \pm\phi_0$) and becomes smaller in front of the wedge ($\phi = \pi$), where in this particular angle the field intensity becomes independent of t_{im}. Since the value of t_{im} can take any negative value, the second factor takes values between 1 and infinity. One interesting limit case is when one considers a perfect metal, and an infinite thin wedge ($\alpha \to 0$), such that $t_{re} \to 0.5$ and $t_{im} \to 0$. In this case, the variation of intensity with ρ can be as strong as $1/\rho$, which is similar to the dependence of intensity on gap size for closely spaced nanostructures in the perfect metal limit.[32] Therefore, the so-called lightning rod effects that can occur with perfect metals are negligible compared to plasmonic effects, where the parameter $t_{re} \to 0$, and the field

dx.doi.org/10.1021/jz200825g |J. Phys. Chem. Lett. 2011, 2, 1978–1983

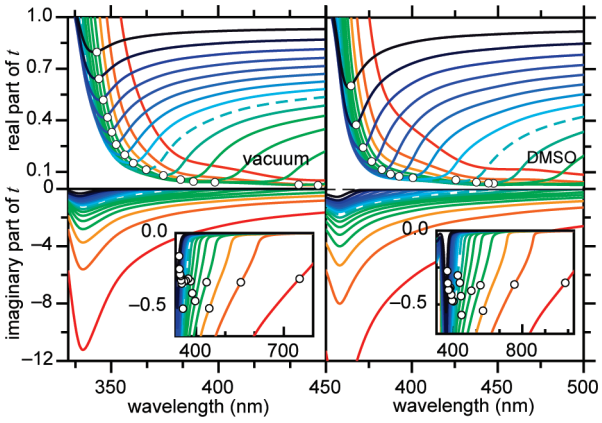

Figure 2. Real (top) and imaginary (bottom) parts of t as a function of the wavelength for Ag wedges immersed in vacuum and DMSO with α from 10° (red line) to 170° (black line) in steps of 10°. Curve for α = 90° is plotted in dashed lines. The minimum values of t_{re} and the corresponding values of t_{im} in the insets are plotted with white circles.

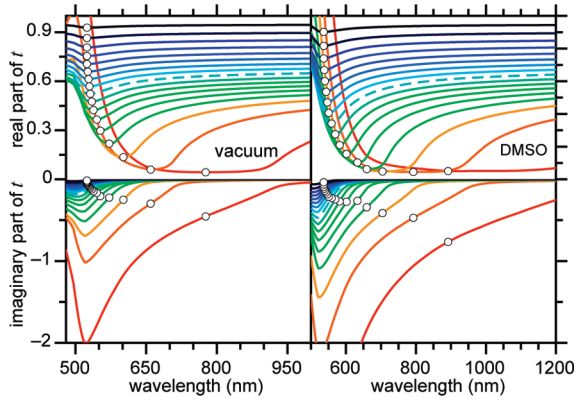

Figure 3. The same as in Figure 2 but for Au wedges.

enhancement can be several orders of magnitude larger, as we discuss below.

Figures 2 and 3 show results for the power index t as a function of the wavelength for Ag and Au wedges, respectively, immersed in vacuum and dimethyl sulfoxide (DMSO). When α = 180°, we have a plane, so $t_{re} = 1$ and $t_{im} = 1$, independently of the material, which means that there is no singularity, as expected for a propagating SPR. We observe that the behavior for a Au wedge is very similar to that found for Ag, with values of t_{re} slightly larger for Au than for Ag. This means that the singularity for Ag is stronger than that for Au, and thus the EM field enhancement. We find that the smaller the wedge angle, the smaller the values of t_{re}, and likewise the stronger the fields. For instance, for a Ag (Au) wedge in vacuum with α = 90°, the minimum $t_{re} = 0.113$ (0.523) is at 365 nm (531 nm), while for a Ag (Au) wedge in vacuum with α = 10°, the minimum $t_{re} = 0.009$ (0.043) is at 754 nm (772 nm). Then, the singularity is 2 (1) orders of magnitude larger for the sharper Ag (Au) wedge, but is also red-shifted by about 400 nm (200 nm). If we consider the wedge immersed in DMSO, the behavior as a function of the angle is the same, but now the minimum values are red-shifted, as expected when the system is in a medium with a larger refractive index. Additionally, t_{re} reaches smaller values, increasing the singularity of the field.

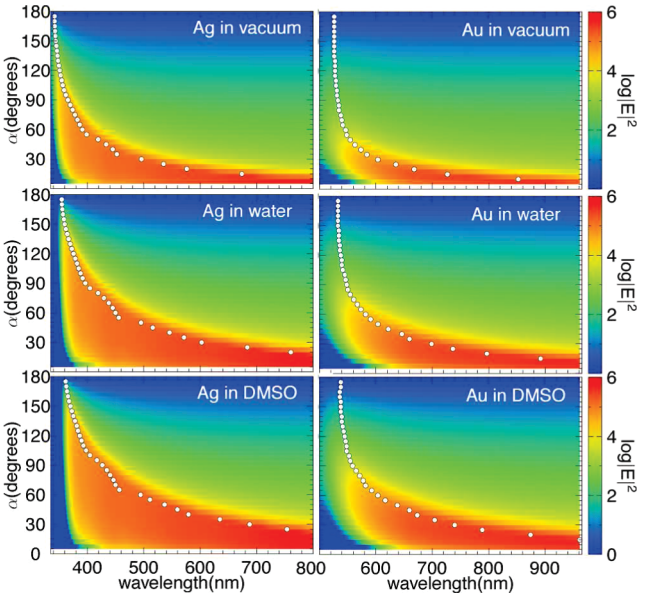

Figure 4. EM field intensities as a function of α and wavelength at ρ = 1 nm, φ = π. White circles show the strongest field. Color bars show the intensity in logarithmic scale. The refraction indexes of the host media are $N = 1$ for vacuum, 1.33 for water, and 1.47 for DMSO.

For example, the Ag (Au) wedge in DMSO with α = 90° has a minimum value of $t_{re} = 0.046$ (0.341) at 424 nm (559 nm), which is 1 order (half) of magnitude smaller than in vacuum, and is red-shifted by about 60 nm (30 nm). For α = 10° the minimum is $t_{re} = 0.007$ (0.051) at 1050 nm (892 nm), which is smaller (larger) than in vacuum but of the same order of magnitude, and now is red-shifted 300 nm (120 nm).

The optimum wedge with the strongest enhancement is not always the sharpest one. For example, at 400 nm the angle for which the strongest field occurs for Ag in vacuum is α = 40°, while in DMSO it is α = 80°. For Au at 600 nm, the angle for which the strongest field occurs in DMSO is α = 50°, while in vacuum it is α = 20°. Additionally, it is found that Au wedges are slightly less sensitive to morphology and environmental changes than Ag ones.

Now, we analyze the imaginary part of the index power parameter. We observe that the values of t_{im} at the wavelengths that correspond to the minima of t_{re} are $0 < t_{im} < 0.7$, such that the second factor on the right-hand side of eq 3 takes values $1 \leq \cosh[2t_{im}(\phi - \pi)] \leq 10$. This means that at a fixed radial distance from the wedge, the intensity of the field varies less than 1 order of magnitude with the angle, being larger near the walls ($\phi \sim \pm\phi_0$), and equal to 1 in front of the wedge ($\phi = \pi$). For Ag, the minimum value of t_{im} is found at about 336 nm in vacuum and 357 nm in DMSO for all angles α. However, at such wavelengths the values of $t_{re} > 1$, which corresponds to the case when there are no singularities, and thus eq 3 is not valid. The same occurs for Au, where now the minimum value of t_{im} is found from 496 to 521 nm in vacuum, and from 508 to 523 in DMSO. Therefore, the main contribution to the EM intensity variation comes from the radial singularity.

To illustrate the contribution of the first factor in the right-hand side of eq 3, the EM field intensity at 1 nm from the tip ($\phi = \pi$) of the wedge is shown in Figure 4 as a function of α and the wavelength. We discuss the case for three different media: vacuum, water, and DMSO. On the left-hand side of Figure 4,

dx.doi.org/10.1021/jz200825g |J. Phys. Chem. Lett. 2011, 2, 1978–1983

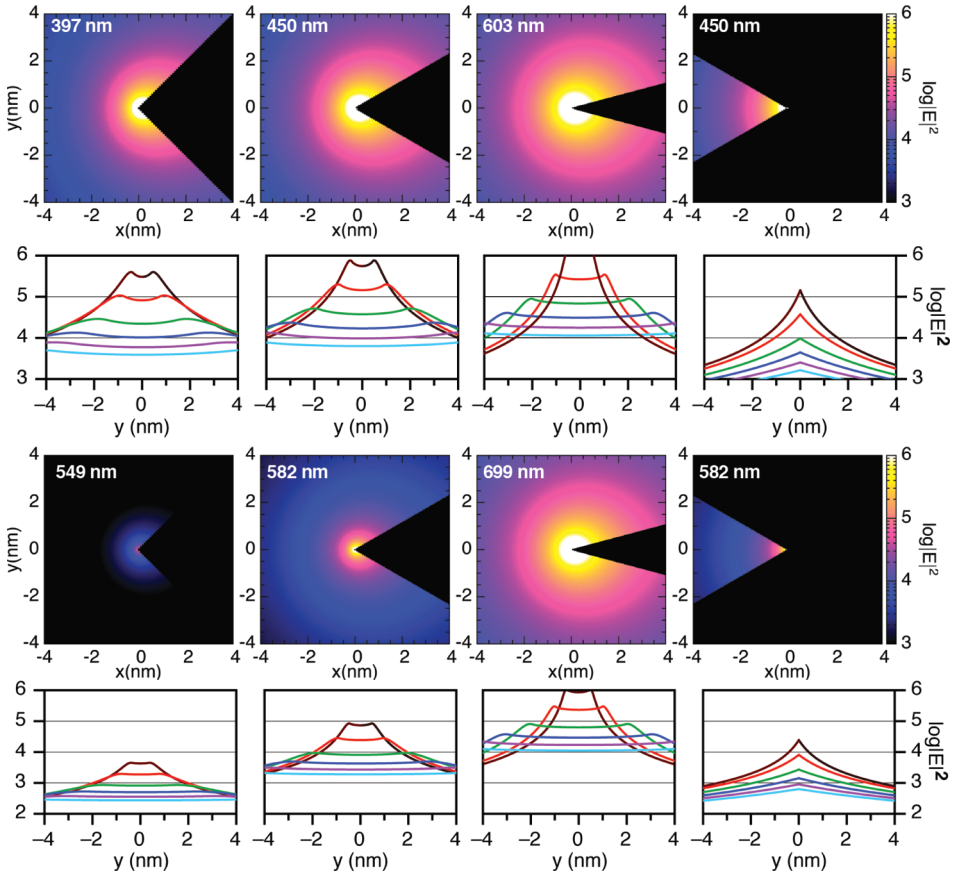

Figure 5. Color maps of the EM field intensities as a function of the position for Ag wedges in water (top) at 397 nm with $\alpha = 90°$, 450 nm with $\alpha = 60°$, 603 nm with $\alpha = 30°$, and a groove at 450 nm and $\alpha = 300°$. Below the color maps, the field intensities for each case are shown as a function of y that follows paths around the wedge at different fixed distances—0.5 (brown), 1 (red), 2 (green), 3 (blue), 4 (purple), and 5 nm (light blue)—as depicted in Figure 1. The same for Au wedges in water (bottom) at 549 nm with $\alpha = 90°$, 582 nm with $\alpha = 60°$, 699 nm with $\alpha = 30°$, and a groove at 582 nm and $\alpha = 300°$. The field intensities for each case are also shown as a function of y, which follow the paths at the same fixed distances.

we show results for Ag, while on the right-hand side results for Au are shown. The color maps are in a logarithmic scale and show the EM field intensity normalized to the incident field, where red corresponds to the strongest EM fields with values 10^6 times the incident field, while blue corresponds to a null enhancement (10^0). For Ag in vacuum, it is observed that the EM enhancements of $\geq 10^4$ occur at small wavelengths over a narrow wavelength range close to 360 nm and then broadening to a much larger wavelength range for sharper wedges ($\alpha \leq 110°$). As the refractive index increases, the internal angle region with EM intensification $\geq 10^4$ also does, for instance, $\alpha \leq 135°$ in water, and $\alpha \leq 145°$ in DMSO. The same happens for Au, but now the largest fields with $\geq 10^4$ start at larger wavelengths ($\sim$ 565 nm), and the internal angles that lead to broader wavelength ranges are below 45° in vacuum, 65° in water, and 75° in DMSO.

We also observe at 1 nm and $\phi = \pi$ in Figure 4 that larger EM field intensities are found for very acute internal angles α, and these values are at large wavelengths, as expected from the behavior of t_{re} shown in Figures 2 and 3. In the case of Ag, the field intensity reaches values up to 10^6 times the incident field in all the host media and $\alpha \leq 10°$, while for Au the maximum is 10^5 times the incident field with $\alpha \leq 25°$ in vacuum, $\alpha \leq 40°$ in water, and $\alpha \leq 50°$ in DMSO. An interesting feature of the wedge is that for small angles α there is an ample region of wavelengths where the intensity is large. For example, a Ag wedge in vacuum with $\alpha = 10°$ shows large field intensities ($\geq 10^5$) from about 530 to 840 nm, while the same wedge immersed in DMSO goes from 660 to 1190 nm. On the other hand, when $\alpha = 90°$, the maximum is about 10^4 in vacuum with a bandwidth of about 25 nm from 350 to 375 nm, which is much smaller than the one observed for $\alpha = 10°$ with a bandwidth of about 300 nm. A similar behavior is observed in other host media, but now the bandwidth becomes larger. For instance, when $\alpha = 90°$ in DMSO an intensity larger than 10^4 is found in a bandwidth of about 80 nm from 370 to 450 nm in contrast with the corresponding case in vacuum with a bandwidth of 25 nm.

The broad continuous resonance band for small values of α is inherent to the geometry of the wedge, being quite distinct from the much narrower plasmon resonances that are found for discrete NPs. This is a useful property for solar energy applications, where enhancements over a broad spectra range covering the solar spectrum are important. Note that for sharp tips like star decahedra, and for the finite TERS tips that have been studied previously using FDTD methods,[17−19] a progression of multipole resonances is found rather than a broad continuum. The overlapping region of these multipoles can also be broad,[13] so in this respect the results are similar. In the TERS work with infinite tips that was mentioned earlier,[21] broad continuous bands similar to that in Figure 4 were found for tip angles $a = 15°$. The smallest radius of curvature considered was 10 nm, and in this case the

dx.doi.org/10.1021/jz200825g |J. Phys. Chem. Lett. 2011, 2, 1978–1983

maximum field intensity was 10^2. While this is much smaller than is found in the present case with a sharp wedge, the behavior with wavelength is otherwise analogous. In the quasistatic prolate ellipsoidal work that was mentioned earlier,[23] there is no concept of an angle α, so comparisons are more difficult. The results show only one strong resonance that red shifts as radius of curvature decreases, so in this respect the results are similar.

Let us analyze the dependence of the EM field intensity with distance to the wedge. We choose the wavelengths where the maximum intensity is found for a given α, and we evaluate the field along the constant d lines in Figure 1. In Figure 5, we show the case for Ag (top) and Au (bottom) wedges immersed in water, including one choice of α where the wedge becomes a groove (right-most panel in the figure). We see that the intensities for Ag are at least 1 order of magnitude larger than those for Au. Additionally, we mentioned above that these intensities are 1 order of magnitude larger for wedges immersed in water than in vacuum. The largest intensity is found for the closest distance to the wedge, the path with $d = 0.5$ nm, and the more acute α. For instance, for $\alpha = 30°$ and $d = 0.5$ nm, the intensity reaches values $\sim 10^7$ for Ag and $\sim 10^6$ for Au. Notice that except for the groove ($\alpha = 300°$) the maximum field intensity does not occur directly in front of the tip ($y = 0$), because at this point $\phi = 0$, and the contribution from t_{im} is minimum in eq 3. On the other hand, for positions close to the walls of the wedge, the cosh term slightly modulates the intensity. However, the most important feature associated with the cosh term in eq 3 is that it creates a region where the maximum field intensity at a given distance is more or less constant, i.e., this shows the possibility to have large enhancements in a region close to the tip, and not only at a single point. Additionally, for acute angles α these plateaus in the intensity become more uniform. The size of the plateaus depends on the distance d; as d increases, the size of the plateau also increases. However, the intensity decays rapidly with increasing d, being larger for Ag than for Au, because t_{re} is always smaller for Ag than for Au. In the case of the groove structure, a rapid decay is always present because the contribution from the cosh term in eq 3 is very small (~ 1) for large angles ($\phi > 300°$), thus the plateaus are not present.

In conclusion, we have shown that localized SPRs at the tip of wedge-shaped noble metal nanostructures increase the EM field intensity several orders of magnitude with respect to the incident field for positions that are 1 nm away from the tip singularity. For a given wavelength, there is an intensity maximum as a function of wavelength, which depends on the host dielectric medium and the internal angle of the wedge. We also find broad wavelength bands of intensity maxima, which become broader as the angle diminishes and the host's refractive index increases. This opens the possibility of generating high field enhancements over a large region of the UV−vis spectrum with an appropriate choice of wedge parameters. These results, which are in accord with more limited results generated previously for TERS tips using finite element calculations, are relevant to the use of a single nanostructure morphology to enhance SERS for measurements that span a broad range of wavelengths. Of course the present study has ignored the effects of quantum tunneling, electronic hopping, non locality, and so forth, which can be present at smaller distances and can hamper the field enhancement compared to what we have calculated.

AUTHOR INFORMATION

Corresponding Author

*E-mail: cecilia@fisica.unam.mx.

ACKNOWLEDGMENT

This work was supported in part by UNAM-DGAPA (PAPIIT IN106408), a grant from the U.S. Department of Energy, Office of Science, Office of Basic Energy Sciences, under Award Number DE-SC0004752, by CONACyT, and the Air Force Office of Scientific Research (SOARD FA9550-09-1-0579). We thank Carlos Roman-Velazquez, Patrick Shively, and Marty Blaber for helpful discussions.

REFERENCES

(1) Maier, S. A.; Kik, P. G.; Atwater, H. A.; Meltzer, S.; Harel, E.; Koel, B. E.; Requicha, A. A. G. Local Detection of Electromagnetic Energy Transport Below the Diffraction Limit in Metal Nanoparticle Plasmon Waveguides. *Nat. Mater.* **2003**, *2*, 229–232.

(2) Camden, J. P.; Dieringer, J. A.; Zhao, J.; Van Duyne, R. P. Controlled Plasmonic Nanostructures for Surface-Enhanced Spectroscopy and Sensing. *Acc. Chem. Res.* **2008**, *41*, 1653–1661.

(3) Jin, R.; Cao, Y.; Mirkin, C.; Kelly, K.; Schatz, G.; Zheng, J.-G. Photo-induced Conversion of Silver Nanospheres to Nanoprisms. *Science* **2001**, *294*, 1901–1903.

(4) Jin, R.; Cao, Y. C.; Hao, E.; Métraux, G. S.; Schatz, G. C.; Mirkin, C. Controlling Anisotropic Nanoparticle Growth Through Plasmon Excitation. *Nature* **2003**, *425*, 487–490.

(5) Atwater, H. A.; Polman, A. Plasmonics for Improved Photovoltaic Devices. *Nat. Mater.* **2010**, *9*, 205–213.

(6) Huang, X.; El-Sayed, I. H.; Qian, W.; El-Sayed, M. A. Cancer Cell Imaging and Photothermal Therapy in the Near-Infrared Region by Using Gold Nanorods. *J. Am. Chem. Soc.* **2006**, *128*, 2115–2120.

(7) Zhang, J. Z.; Noguez, C. Plasmonic Optical Properties and Applications of Metal Nanostructures. *Plasmonics* **2008**, *3*, 127–150.

(8) Noguez, C. Surface Plasmons on Metal Nanoparticles: The Influence of Shape and Physical Environment. *J. Phys. Chem. C* **2007**, *111*, 3806–3819.

(9) Ferry, V. E.; Munday, J. N.; Atwater, H. A. Design Considerations for Plasmonic Photovoltaics. *Adv. Mater.* **2010**, *22*, 4794–4808.

(10) Moskovits, M. Surface-Enhanced Spectroscopy. *Rev. Mod. Phys.* **1985**, *57*, 783–826.

(11) Hartschuh, A.; Beversluis, M. R.; Bouhelier, A.; Novotny, L. Tip-Enhanced Optical Spectroscopy. *Philos. Trans. R. Soc. London, A* **2004**, *362*, 807–819.

(12) Sherry, L. J.; Jin, R. C.; Mirkin, C. A.; Schatz, G. C.; Van Duyne, R. P. Localized Surface Plasmon Resonance Spectroscopy of Single Silver Triangular Nanoprisms. *Nano Lett.* **2006**, *6*, 2060–2065.

(13) González, A. L.; Noguez, C. Influence of Morphology on the Optical Properties of Metal Nanoparticles. *J. Comput. Theor. Nanosci.* **2007**, *4*, 231–238.

(14) González, A. L.; Noguez, C. Optical Properties of Silver Nanoparticles. *Phys. Status Solidi C* **2007**, *4*, 4118–4126.

(15) Davis, L. C. Electostatic Edge Modes of a Dielectric Wedge. *Phys. Rev. B* **1976**, *14*, 5523–5525.

(16) Micic, M.; Klymyshyn, N.; Suh, Y. D.; Lu, H. P. Finite Element Method Simulation of the Field Distribution for AFM Tip Enhanced Surface-Enhanced Raman Scanning Microscopy. *J. Phys. Chem. B* **2003**, *107*, 1574–1584.

(17) Roth, R. M.; Panoiu, N. C.; Adams, M. M.; Osgood, R. M. Resonant-Plasmon Field Enhancement from Asymmetrically Illuminated Conical Metallic-Probe Tips. *Opt. Express* **2006**, *14*, 2921–2931.

(18) Sukharev, M.; Seideman, T. Optical Properties of Metal Tips for Tip-Enhanced Spectroscopies. *J. Phys. Chem. A* **2009**, *113*, 7508–7513.

(19) Yang, Z.; Aizpurua, J.; Xu, H. Electromagnetic Field Enhancement in TERS Configurations. *J. Raman Spectrosc.* **2009**, *40*, 1343–1348.

(20) Demming, A. L.; Festy, F.; Richards, D. Plasmon Resonances on Metal Tips: Understanding Tip-Enhanced Raman Scattering. *J. Chem. Phys.* **2005**, *122*, 184716−1–184716−7.

(21) Zhang, W.; Cui, X.; Martin, O. J. Local Field Enhancement of an Infinite Conical Metal Tip Illuminated by a Focused Beam. *J. Raman Spectrosc.* **2009**, *40*, 1338–1342.
(22) Pettinger, B.; Domke, K. F.; Zhang, D.; Picardi, G.; Schuster, R. Tip-Enhanced Raman Scattering: Influence of the Tip-Surface Geometry on Optical Resonance and Enhancement. *Surf. Sci.* **2009**, *603*, 1335–1341.
(23) Behr, N.; Raschke, M. B. Optical Antenna Properties of Scanning Probe Tips: Plasmonic Light Scattering, Tip-Sample Coupling, and Near-Field Enhancement. *J. Phys. Chem. C* **2008**, *112*, 3766–3773.
(24) Meixner, J. The Behavior of Electromagnetic Fields at Edges. *IEEE Trans. Antennas Propag.* **1972**, *20*, 442–446.
(25) Novotny, L.; Bian, R. X.; Xie, X. S. Theory of Nanometric Optical Tweezers. *Phys. Rev. Lett.* **1997**, *79*, 645–648.
(26) Lapchuk, A. S.; Shylo, S. A.; Nevirkovets, I. P. Local Plasmon Resonance at Metal Wedge. *J. Opt. Soc. Am. A* **2008**, *25*, 1535–1540.
(27) Johnson, P. B.; Christy, R. W. Optical Constants of the Noble Metals. *Phys. Rev. B* **1972**, *6*, 4370–4379.
(28) Dobrzynski, L.; Maradudin, A. A. Electrostatic Edge Modes in a Dielectric Wedge. *Phys. Rev. B* **1972**, *6*, 3810–3815.
(29) García de Abajo, F. J.; Aizpurua, J. Numerical Simulation of Electron Energy Loss Near Inhomogeneous Dielectrics. *Phys. Rev. B* **1997**, *56*, 15873–15884.
(30) We are studying the asymmetric mode as the oscillations in electric polarization are antisymmetric with respect to the symmetry plane. However, it can also be considered as the symmetric mode as the H field is symmetric.
(31) Talisa, S. Application of Davidenko's Method to the Solution of Dispersion Relations in Lossy Waveguiding Systems. *IEEE Trans.: Microwave Theory and Techniques* **1985**, *33*, 967–971.
(32) McMahon, J. M.; Gray, S. K.; Schatz, G. C. Fundamental Behavior of Electric Field Enhancements in the Gaps Between Closely Spaced Nanostructures. *Phys. Rev. B* **2011**, *83*, 115428−1–115428−15.